Synchronization Stability Analysis Based on Dual-Sequence Dynamic Coupling Model for Grid-Following Inverters Under Asymmetrical Grid Faults

Jingrong Yu, Wenhao Yang, Jiaqi Yu, Chen Peng, Tingyi Jiang, and Hankang Tian

***Abstract*—To deal with asymmetrical grid faults, grid-following inverters are required to output positive- and negative-sequence currents to regulate the voltage at the point of common coupling. Owing to the negative-sequence current injection, the stability mechanism of the dual-sequence synchronizations becomes more complicated under asymmetrical scenarios. In this article, a dual-sequence dynamic coupling model, which takes into account both positive- and negative-sequence current couplings as well as power angle difference, is proposed. Based on this model, not only the existence conditions of positive- and negative-sequence equilibrium points are identified, but also the transient process stability conditions of the operating points are determined, resulting in a complete transient stability judgment foundation during asymmetrical grid faults. It is pointed out that couplings between the positive- and negative-sequence synchronization processes bring about more transient synchronization instability. Simulation and experimental results verify that the proposed synchronization stability analysis based on the dual-sequence dynamic coupling model has higher accuracy for inverters under asymmetrical grid faults compared with the previous methods.**

***Index Terms*—Asymmetrical grid faults, dual-sequence current regulation, grid-following inverters, transient synchronization stability.**

I. Introduction

With the increasing penetration of renewable power generation, a new power system with renewable energy as the dominant power source has emerged in many countries [1], [2], [3]. According to practical statistics, asymmetrical short-circuit faults have a probability of occurrence of up to 90% [4], [5] of all the short-circuit faults, resulting in unbalanced voltage sags and voltage instability. To assure the voltage stability of the new power system in the face of asymmetrical grid faults, the latest grid codes put forward a dual-sequence current injection requirement for grid-connected inverters in grid-following control mode [6].

However, the dual-sequence current injection leads to a higher risk of synchronization instability for inverters [7], [8]. Since both positive- and negative-sequence output currents must be synchronized with the grid, the inverters with dual-sequence currents are more susceptible to synchronization instability. From the perspective of the presence of the equilibrium points and the transient process stability of the operating points, the synchronization stability of the inverters with dual-sequence current injection is generally studied. First, the absence of equilibrium points implies instability. The stability analysis in [9], taking the positive- and negative-sequence current couplings into account, mainly focuses on the existence of steady-state equilibrium points and identifies the type of instability. Nevertheless, little attention is paid to the dynamic behavior of the operating points during the faults. Similarly, Taul et al. [10] did not give the determination conditions for the operating points to reach stable equilibrium points after a dynamic transition and it neglects the couplings of positive- and negative-sequence currents in the described stable conditions.

Meanwhile, even when equilibrium points exist, synchronization instability may also occur in grid-connected inverters. Based on energy conservation, Li et al. [11] discussed whether the original equilibrium point could shift to a new available equilibrium point under asymmetric faults without losing transient stability. Unfortunately, Li et al. [11] entirely disregarded the coupling impacts of positive- and negative-sequence currents. It is worth mentioning that the couplings of dual-sequence currents can only be totally eliminated when the fault point is located extremely close to the infinite bus. In fact, the location where the fault occurs is arbitrary, and when the fault point is located far from the infinite bus, the couplings of positive and negative sequences are so large that the coupling currents cannot be neglected. Therefore, it is obviously not universal to completely ignore the couplings between the positive- and negative-sequence synchronizations.

Received 5 June 2024; revised 19 August 2024; accepted 2 October 2024. Date of publication 11 October 2024; date of current version 18 December 2024. This work was supported in part by the Natural Science Foundation of Hunan Province under Grant 2022JJ30742 and in part by the Natural Science Foundation of China under Grant 52207076. Recommended for publication by Associate Editor G. D. Donato. *(Corresponding author: Jiaqi Yu.)*

Jingrong Yu, Wenhao Yang, Chen Peng, Tingyi Jiang, and Hankang Tian are with the School of Automation, Central South University, Changsha 410017, China (e-mail: jingrong@csu.edu.cn; ywh1105@csu.edu.cn; peng.chen@csu.edu.cn; jiangty@csu.edu.cn; tianhankang@csu.edu.cn).

Jiaqi Yu is with the College of Electronic Information and Electrical Engineering, Changsha University, Changsha 410017, China (e-mail: z20190101@ccsu.edu.cn).

Color versions of one or more figures in this article are available at https://doi.org/10.1109/TPEL.2024.3478383.

Digital Object Identifier 10.1109/TPEL.2024.3478383

TABLE I
COMPARISON OF METHODS UNDER ASYMMETRICAL FAULTS

Methods	Transient process	Dual-sequence coupling effects	Dynamics between the dual sequences
[9]	×	√	×
[10]	×	×	×
[11]	√	×	×
[12],[13]	√	√	×
Proposed method	√	√	√

Moreover, ignoring the difference between the positive- and negative-sequence power angles will also limit the accuracy of the synchronization stability. Luo et al. [12] analyzed the synchronization stability of inverters during asymmetrical faults by partly considering the couplings. Yet it is assumed that the phase angle of the negative sequence is equal to the opposite positive-sequence phase angle. Although the coupling effects of positive- and negative-sequence currents are taken into account, the dynamic effect caused by the different phase angles of the positive and the negative sequences is neglected. Similarly, Li et al. [13] also fail to give full consideration to the dynamics of phase angles produced by phase-locked loops (PLLs). In fact, the power angles of the positive and the negative sequences are not always opposite.

A comparison of synchronization stability analysis methods under asymmetrical faults is given in Table I. It is obvious that the present work on the synchronization stability of grid-connected inverters during asymmetrical grid faults is incomplete enough, and the instability mechanism is still unclear. There is currently a lack of synchronization stability analysis, which considers both the couplings and dynamic impacts of positive and negative sequences.

Thereby, this article aims to reveal the influences of positive- and negative-sequence couplings and the effects of dynamics on synchronization stability. The main contributions are summarized as follows.

1) A dual-sequence synchronous dynamic model is constructed, including the coupling effects of positive- and negative-sequence currents. Unlike the models in [10] and [11], which ignore the dual-sequence couplings, the model proposed here takes the dual-sequence coupling effects into consideration and focuses on the grid fault that is located far from the infinite bus.
2) The power angle difference between the positive and negative sequence is pointed out in the proposed model. In contrast to the schemes in [12] and [13] with the assumption that the power angle of negative sequence is opposite to the angle of positive sequence, we here further take the different dynamics between the dual-sequence angles into account. By considering the couplings and the power angle difference between the dual sequences, the proposed model gives a complete description of synchronization behaviors with dual-sequence output currents.

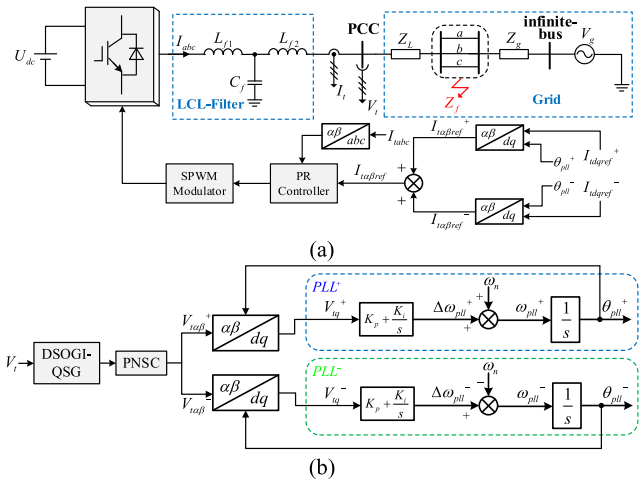

Fig. 1. Inverter topology and control scheme. (a) Dual-sequence current regulation. (b) Dual-sequence synchronization.

3) A method for transient stability judgment under asymmetrical faults is proposed. Compared with the conventional schemes in [9] and [10], the proposed method not only judges the existence of positive- and negative-sequence equilibrium points but also includes transient process stability conditions, giving more accurate transient stability results.

The rest of the article is structured as follows. In Section II, the structure and control scheme of the inverter with dual-sequence synchronization are presented. In Section III, a dual-sequence synchronous dynamic model considering positive- and negative-sequence current couplings and power angle difference is constructed. In Section IV, a complete dual-sequence transient stability analysis method is proposed. Simulation and experimental results are given in Section V. Finally, Section VI concludes this article.

II. POSITIVE- AND NEGATIVE-SEQUENCE SYNCHRONIZATIONS DURING ASYMMETRICAL GRID FAULTS

A. Structure and Control Scheme of the Inverter

The topology and control scheme of the inverter studied in this article are shown in Fig. 1. $U_{\rm dc}$ represents the dc-link voltage. The current vector injected into the grid is I_t, and V_t and V_g represent the point of common coupling (PCC) voltage and the grid voltage, respectively. If an asymmetrical grid fault occurs between the PCC and the infinite bus, then the equivalent impedance from the PCC to the fault point is denoted by Z_L, and the equivalent impedance from the fault point to the grid is denoted by Z_g.

The control scheme can be divided into two parts, the dual-sequence synchronization and the dual-sequence current regulation. The dual-sequence synchronization mainly consists of the dual-sequence separator and dual-sequence PLL$^+$ and PLL$^-$. First, the quadrature signals are obtained by the dual second-order generalized integrator-quadrature signal generator, and

then computed by the positive- and negative-sequence computation (PNSC) [10], [11], [14]. Ultimately, the positive- and negative-sequence components of the PCC voltage, $V_{t\alpha\beta}{}^{+}$ and $V_{t\alpha\beta}{}^{-}$, are separated. The dual-sequence PLLs aim to extract the positive- and negative-sequence phase angles for the control of the dual-sequence currents.

In Fig. 1, $\omega_{\rm pll}{}^{+}$ and $\omega_{\rm pll}{}^{-}$ denote the positive- and negative-sequence angular frequencies, whereas $\theta_{\rm pll}{}^{+}$ and $\theta_{\rm pll}{}^{-}$ denote the positive- and negative-sequence phase angles. It is assumed that the grid frequency is maintained at the rated angular frequency ω_n. For the dual-sequence current regulation, the PR control is selected, and only two PR controllers are required [10], [15].

$I_t{}^{+}$ and $I_t{}^{-}$ denote the positive- and negative-sequence components of the current I_t injected into the grid, respectively

$$\begin{cases} I_t^{+} = \left|I_t^{+}\right| e^{j\left(\theta_{\rm pll}^{+}+\theta_I^{+}\right)} \\ I_t^{-} = \left|I_t^{-}\right| e^{j\left(\theta_{\rm pll}^{-}+\theta_I^{-}\right)} \end{cases} \tag{1}$$

where $\theta_I{}^{+}$ and $\theta_I{}^{-}$ denote the angles of the positive- and negative-sequence current vectors to the d^{+}/d^{-} rotating reference frames, respectively, given by $\theta_I{}^{+} = \arctan\left(I_{tq}{}^{+}/I_{td}{}^{+}\right)$ and $\theta_I{}^{-} = \arctan\left(I_{tq}{}^{-}/I_{td}{}^{-}\right)$.

$I_{td}{}^{+}/I_{tq}{}^{+}$ and $I_{td}{}^{-}/I_{tq}{}^{-}$ denote the d^{+}/q^{+}-axis components of $I_t{}^{+}$ and d^{-}/q^{-}-axis components of $I_t{}^{-}$. $I_{td\rm ref}{}^{+}/I_{tq\rm ref}{}^{+}$ and $I_{td\rm ref}{}^{-}/I_{tq\rm ref}{}^{-}$ represent the active/reactive reference values of positive- and negative-sequence currents $I_t{}^{+}/I_t{}^{-}$ injected into the grid, respectively, which are specified during asymmetrical grid faults. It should be noted that the d^{+}/q^{+} axis rotates counterclockwise with the angular speed of $\omega_{\rm pll}{}^{+}$, whereas the d^{-}/q^{-} axis rotates clockwise with the angular speed of $\omega_{\rm pll}{}^{-}$.

For transient stability analysis under asymmetrical grid faults, some assumptions should be considered, which have been widely adopted in previous research [9], [10], [11], [13], [16], [17].

1) The dc-link voltage $U_{\rm dc}$ is approximated as a constant. Since the dc side of the inverter is assumed to be controlled by another converter independently, the influence of the dc-link control loop on the synchronization stability can be neglected.
2) The model of the inverter can be considered to be an ideal controllable current source, with the parallel equivalent impedance being neglected. The transient stability problem is limited to the low-frequency range where the inverter's parallel equivalent impedance is assumed to be infinite due to the grid-following control mode with the fast control of output current.
3) The current reference values $I_{td\rm ref}{}^{+}/I_{tq\rm ref}{}^{+}$ and $I_{td\rm ref}{}^{-}/I_{tq\rm ref}{}^{-}$ can be immediately tracked by $I_{td}{}^{+}/I_{tq}{}^{+}$ and $I_{td}{}^{-}/I_{tq}{}^{-}$. Since the bandwidth of the dual-sequence synchronization is much lower than that of the current controller, the current control dynamics can be ignored when analyzing transient stability.

B. Equivalent Circuit of the Sequence Networks

For the subsequent synchronization stability analysis, it is necessary to derive the positive- and negative-sequence expressions of PCC voltage. There are three typical asymmetrical short-circuit faults, i.e., single line-to-ground (SLG), double line-to-ground (DLG), and line-to-line (LL). Their boundary conditions are given in Fig. 2. According to these conditions, the positive, negative, and zero sequence networks of the system can be linked to form the equivalent circuit in Fig. 3 [9], [11]. Compared with symmetrical scenarios, the major difference is that dual-sequence currents are both incorporated in the interconnected sequence networks [10].

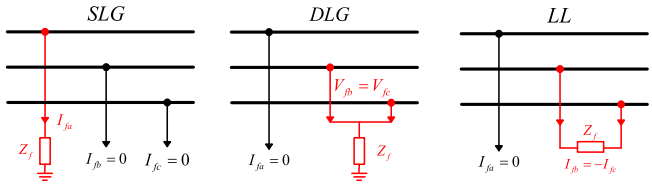

Fig. 2. Three types of short-circuit faults and their boundary conditions.

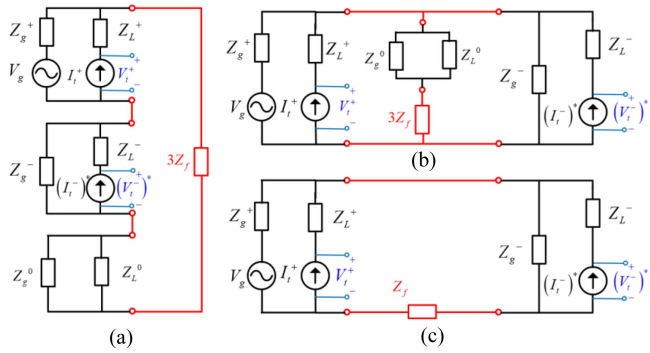

Fig. 3. Equivalent circuit of the sequence networks. (a) SLG. (b) DLG. (c) LL.

$V_t{}^{+}$ and $V_t{}^{-}$ are the positive- and negative-sequence voltages at the PCC. Grid voltage is balanced and exists only in the positive-sequence network. $Z_m{}^{+}$, Z_m, and $Z_m{}^{0}$, where $m = g, L$ denote the positive-sequence, negative-sequence, and zero-sequence components of the line impedances, respectively.

Based on the equivalent circuit in Fig. 3, the positive- and negative-sequence expressions for the PCC voltage under the effects of grid voltage, positive-sequence current, and negative-sequence current can be derived as

$$\begin{cases} V_t^{+} = K_1 V_g + \left(Z_g^{+} K_1 + Z_L^{+}\right) I_t^{+} + Z_g^{+} K_4 (I_t^{-})^{*} \\ (V_t^{-})^{*} = K_4 V_g + \left(Z_g^{-} K_1 + Z_L^{-}\right) (I_t^{-})^{*} + Z_g^{+} K_4 I_t^{+} \end{cases}. \tag{2}$$

After making a unification of the impedance-correlated terms of (2), we get

$$\begin{cases} V_t^{+} = K_1 V_g + Z_2 I_t^{+} + Z_3 (I_t^{-})^{*} \\ (V_t^{-})^{*} = K_4 V_g + Z_5 (I_t^{-})^{*} + Z_6 I_t^{+} \end{cases} \tag{3}$$

where $Z_2 = Z_g^{+} K_1 + Z_L^{+} = |Z_2| \angle \phi_2$, $Z_3 = Z_g^{+} K_4 = |Z_3| \angle \phi_3$, $Z_5 = Z_g^{-} K_1 + Z_L^{-} = |Z_5| \angle \phi_5$, $Z_6 = Z_g^{+} K_4 = |Z_6| \angle \phi_6$. Table II shows the expressions of K_1 and K_4 under different grid faults.

TABLE II
K_1 AND K_4 UNDER DIFFERENT GRID FAULTS

Faults	$K_1 = \lvert K_1\rvert \angle\phi_1$	$K_4 = \lvert K_4\rvert \angle\phi_4$
SLG	$\dfrac{Z_g^- + Z_g^0 // Z_L^0 + 3Z_f}{Z_g^+ + Z_g^- + Z_g^0 // Z_L^0 + 3Z_f}$	$\dfrac{-Z_g^-}{Z_g^+ + Z_g^- + Z_g^0 // Z_L^0 + 3Z_f}$
DLG	$\dfrac{Z_g^0 // Z_L^0 + 3Z_f}{Z_g^+ + 2\left(Z_g^0 // Z_L^0\right) + 6Z_f}$	$\dfrac{Z_g^0 // Z_L^0 + 3Z_f}{Z_g^+ + 2\left(Z_g^0 // Z_L^0\right) + 6Z_f}$
LL	$\dfrac{Z_g^- + Z_f}{Z_g^+ + Z_g^- + Z_f}$	$\dfrac{Z_g^-}{Z_g^+ + Z_g^- + Z_f}$

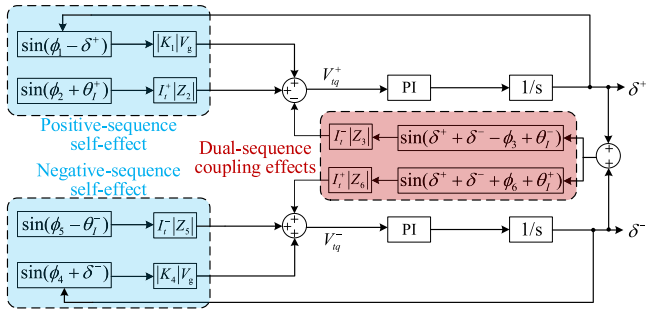

Fig. 4. Diagram for the description of dual-sequence coupling effects.

III. SYNCHRONOUS DYNAMIC MODEL CONSIDERING DUAL-SEQUENCE COUPLINGS AND POWER ANGLE DIFFERENCE

A. Dual-Sequence Couplings and Power Angle Difference

During symmetrical faults, the phase difference between the PCC voltage and the grid voltage is called the power angle [18], [19], [20]. However, under asymmetrical grid faults, the PCC voltage includes positive- and negative-sequence components. So, there are two kinds of power angles for the inverter. Considering that the phase of the grid voltage is θ_g, the positive-sequence power angle is defined as the phase difference between the PCC positive-sequence voltage and the grid voltage, i.e., $\delta^+ = \theta_{\text{pll}}{}^+ - \theta_g$, and the negative-sequence power angle is the sum of the phases of the PCC negative-sequence voltage and the grid voltage, i.e., $\delta^- = \theta_{\text{pll}}{}^- + \theta_g$.

As shown in Fig. 1, the dynamics of PLL$^+$ and PLL$^-$ depend on $V_{tq}{}^+$ and $V_{tq}{}^-$, which are defined as the q^+/q^--axis components of the positive- and negative-sequence voltages at the PCC

$$\begin{cases} V_{tq}^+ = |K_1|\,|V_g|\sin(\phi_1 - \delta^+) + |Z_2|\left|I_t^+\right|\sin(\phi_2 + \theta_I^+) \\ \quad \underbrace{-|Z_3|\left|I_t^-\right|\sin(\overbrace{\delta^+ + \delta^-}^{\text{dynamic part}} - \phi_3 + \theta_I^-)}_{\text{negative sequence coupling part}} \\ V_{tq}^- = |K_4|\,|V_g|\sin(\phi_4 + \delta^-) + |Z_5|\left|I_t^-\right|\sin(\phi_5 - \theta_I^-) \\ \quad \underbrace{+|Z_6|\left|I_t^+\right|\sin(\overbrace{\delta^+ + \delta^-}^{\text{dynamic part}} + \phi_6 + \theta_I^+)}_{\text{positive sequence coupling part}} \end{cases}. \tag{4}$$

It can be clearly seen that $V_{tq}{}^+$ and $V_{tq}{}^-$ are comprised of two parts, the positive/negative-sequence self-effect and the dual-sequence coupling effects. The negative-sequence current $I_t{}^-$ has a coupling effect on $V_{tq}{}^+$, and $V_{tq}{}^-$ is also influenced by the positive-sequence current $I_t{}^+$. Based on $\theta_I{}^+$, $\theta_I{}^-$, and Park transformation, $I_t{}^+$ and $I_t{}^-$ can be further transformed to $I_{td}{}^+/I_{tq}{}^+$ and $I_{td}{}^-/I_{tq}{}^-$ in the PLL model.

The positive- and negative-sequence currents are verified to be coupled in the low-frequency domain. During asymmetrical grid faults, both the positive- and negative-sequence synchronizations should be considered simultaneously, due to the dual-sequence current injection requirement [11]. Additionally, it is known that the sequence networks are interconnected under asymmetrical scenarios [9]. Therefore, there is a coupling relationship between the positive- and negative-sequence components [21].

If an asymmetrical fault occurs close to the infinite bus, then Z_g will be small, and the values of $|Z_3|$ with respect to $|Z_2|$ and $|Z_6|$ with respect to $|Z_5|$ are quite small, so that the correlation terms of $|Z_3|$ and $|Z_6|$ can be ignored. So, the coupling effects of the dual-sequence currents are completely removed. However, the location of the fault is arbitrary. When the fault occurs far from the infinite bus, Z_g will be very large, and the relevant terms about $|Z_3|$ and $|Z_6|$ cannot be ignored. Then, the coupling effects are very large. Therefore, it is obviously impractical to completely ignore the dual-sequence current coupling effects.

Hence, this article explores the influence of dual-sequence couplings on synchronization stability. To present dual-sequence coupling effects more intuitively, a diagram including the positive/negative-sequence self-effect and the dual-sequence coupling effects is given in Fig. 4.

It is of interest to note that the sum of the positive- and negative-sequence power angles ($\delta^+ + \delta^-$), under the synchronous dynamic influence of PLL$^+$ and PLL$^-$, has a time-varying characteristic. It acts on both the positive- and negative-sequence coupling components and then produces a dynamic influence.

Actually, the power angle of the negative sequence is not opposite to the angle of the positive sequence. It is pointed out that the dynamic power angles of the positive and negative sequences should be considered because of the lower bandwidth of the PLL than the current control loops [16], [22], [23]. To verify this point, Fig. 5 shows the dynamic change of positive- and negative-sequence power angles during asymmetrical faults. In Fig. 5, a single-phase grounded short-circuit fault occurs at 0.5 s, with positive- and negative-sequence currents injected at 1 s and 1.5 s, respectively. It can be seen that the sum of dual-sequence power angles is never equal to zero.

B. Dual-Sequence Synchronous Dynamic Model

According to Fig. 1(b), the dynamics of the positive-sequence PLL and negative-sequence PLL can be obtained as

$$\begin{cases} \dfrac{d\omega_{\text{pll}}^+}{dt} = k_p \dfrac{dV_{tq}^+}{dt} + k_i V_{tq}^+ \\ \dfrac{d\omega_{\text{pll}}^-}{dt} = k_p \dfrac{dV_{tq}^-}{dt} + k_i V_{tq}^- \end{cases}. \tag{5}$$

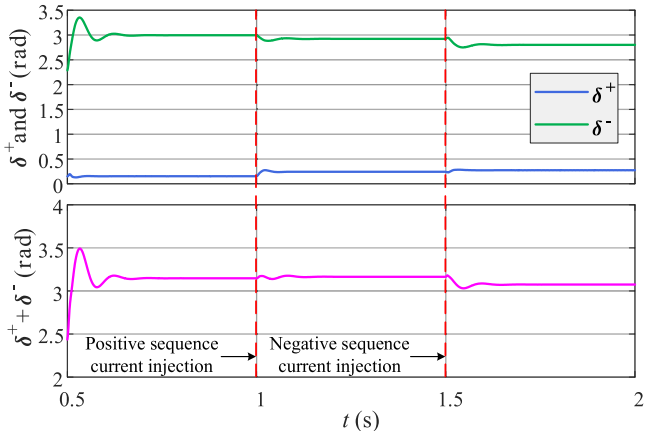

Fig. 5. Dynamics of positive- and negative-sequence power angles during asymmetrical faults.

To better understand the dynamics of dual-sequence PLLs from the physical sight, it is necessary to transform the dynamic equations of PLLs to be equivalent to the rotor equation of synchronous generators [24], [25], [26]. The rotor swing equation of synchronous generators is

$$J\frac{d\omega_{\text{pll}}}{dt} = P^* - P - D\left(\omega_{\text{pll}} - \omega_n\right) \tag{6}$$

where J and D denote inertial and damping coefficients in the rotor swing equation, respectively, and P^* and P are the active power reference and the actual active power output, respectively.

Combined with the expression of $V_{tq}{}^+$ and the dynamic equation of PLL$^+$ in (5), the virtual inertia and damping of PLL$^+$ can be derived based on the standard rotor swing (6). The positive-sequence synchronous dynamic equation of the system can be deduced as

$$J_{v+}^{+}\frac{d\omega_{\text{pll}}^{+}}{dt} - J_{v+}^{-}\frac{d\omega_{\text{pll}}^{-}}{dt} = T_{v+}^{*} - T_{v+} - D_{v+}^{+}(\omega_{\text{pll}}^{+} - \omega_n) + D_{v+}^{-}\left(\omega_{\text{pll}}^{-} + \omega_n\right)$$

$$\begin{cases} T_{v+}^{*} = R_2 I_{\text{tq}}^{+} + \omega_n L_2 I_{td}^{+} - R_3 I_t^{-}\sin\left[(\delta^+ + \delta^-) + \theta_I^-\right] \\ \quad -\omega_n L_3 I_t^{-}\cos\left[(\delta^+ + \delta^-) + \theta_I^-\right] \\ T_{v+} = V^+\sin\left(\delta^+ - \phi_1\right) \\ J_{v+}^{+} = \frac{1 - k_p L_2 I_{td}^{+}}{k_i} \\ J_{v+}^{-} = \frac{k_p}{k_i} L_3 I_t^{-}\cos\left[(\delta^+ + \delta^-) + \theta_I^-\right] \\ D_{v+}^{+} = \frac{k_p}{k_i} V^+\cos\left(\delta^+ - \phi_1\right) - L_2 I_{td}^{+} \\ \quad + \frac{k_p}{k_i} Z_3 I_t^{-}\cos\left[(\delta^+ + \delta^-) + \theta_I^- - \phi_3\right] \\ D_{v+}^{-} = L_3 I_t^{-}\cos\left[(\delta^+ + \delta^-) + \theta_I^-\right] \\ \quad - \frac{k_p}{k_i} Z_3 I_t^{-}\cos\left[(\delta^+ + \delta^-) + \theta_I^- - \phi_3\right] \end{cases} \tag{7}$$

where R_i and L_i, $i = 2, 3$, represent the resistance and inductance values of the impedance Z_i, respectively, and $V^+ = |K_1||V_g|$. It should be noted that the equivalence between the PLL parameters and the rotor equation has been shown in (7). The virtual inertia J_{v+}^{+} and J_{v+}^{-} and the virtual damping D_{v+}^{+} and D_{v+}^{-} are dependent on PLL parameters k_p and k_i.

In (7), T_{v+}^{*} and $T_{\text{v}+}$ denote the positive-sequence virtual prime mover torque and electromagnetic torque, respectively. It should be noted that T_{v+}^{*} includes dq-axis components of the positive-sequence current I_{td}^{+} and I_{tq}^{+}, as well as the coupling effect of the negative-sequence current I_t^-. This coupling effect has a dynamic impact due to the difference in the sum of the positive- and negative-sequence power angles ($\delta^+ + \delta^-$).

J_{v+}^{+} and D_{v+}^{+} are positive-sequence self-effects, representing positive-sequence virtual inertia and damping, respectively. But D_{v+}^{+} includes the dynamic coupling effect of the negative-sequence current I_t^-. J_{v+}^{-} and D_{v+}^{-} are the coupling effects of negative sequence on positive sequence, representing the negative-sequence coupling virtual inertia and damping.

In the same way, combined with the expression of $V_{tq}{}^-$ and the dynamic equation of PLL$^-$ in (5), the negative-sequence synchronous dynamic equation of the system can be derived as (8) shown at the bottom of the next page, where R_i and L_i, $i = 5, 6$, represent the resistance and inductance values of the impedance Z_i, respectively, and $V^- = |K_4||V_g|$.

In (8), T_{v-}^{*} and T_{v-} denote the negative-sequence virtual prime mover torque and electromagnetic torque, respectively. It should be noted that T_{v-}^{*} includes dq-axis components of the negative-sequence current I_{td}^{-} and I_{td}^{-}, as well as the coupling effect of the positive-sequence current I_t^+. This coupling effect has a dynamic characteristic due to the difference in the sum of the positive- and negative-sequence power angles ($\delta^+ + \delta^-$).

J_{v-}^{-} and D_{v-}^{-} are negative-sequence self-effects, representing negative-sequence virtual inertia and damping, respectively. But D_{v-}^{-} includes the dynamic coupling effect of the positive-sequence current I_t^+. J_{v-}^{+} and D_{v-}^{+} are the coupling effects of positive sequence on negative sequence, representing the positive-sequence coupling virtual inertia and damping.

From above, it can be seen that the positive- and negative-sequence synchronous dynamics (7) and (8) take into account the coupling influences of dual-sequence currents and the dynamic effects brought by the difference of dual-sequence power angles.

To show the influences of the dynamic couplings more intuitively, based on (7) and (8), a dual-sequence synchronous dynamic model is constructed in Fig. 6. On the one hand, the input variables T_{v+}^{*} and T_{v-}^{*} directly include the coupling currents and dynamic characteristics. On the other hand, the dynamic coupling influences are constructed in the forms of virtual inertia and damping. To this end, the dynamic interaction effects of the dual-sequence synchronization must be considered when analyzing the synchronization stability, which is quite complex and difficult.

IV. Positive- and Negative-Sequence Synchronization Stability Analysis

The existence of dual-sequence equilibrium points is a prerequisite for the system to remain stable during asymmetrical faults. However, even if the existence criterion is satisfied, the

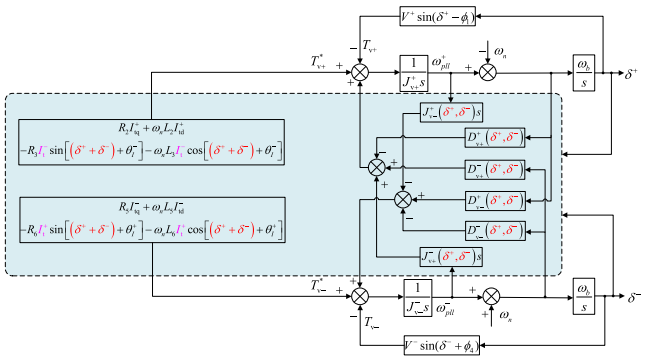

Fig. 6. Dual-sequence synchronous dynamic model considering dual-sequence current couplings and power angle difference.

system may still lose synchronism due to poor dynamic behavior [27]. Therefore, in this section, the dual-sequence synchronous dynamic equations will be further modified for synchronization stability analysis, which consists of two main aspects: 1) the existence of dual-sequence equilibrium points, and 2) the transient characteristics.

A. Dual-Sequence Synchronous Dynamic Equations Considering Dual-Sequence Couplings and Dynamic Effects

Due to the dual-sequence coupling effects, (7) and (8) are different from the swing equation of synchronous generators. It is difficult to directly use them for synchronization stability analysis. Therefore, the relationship between the positive- and negative-sequence frequencies needs to be established to rewrite the dual-sequence synchronous dynamic equations for the standard form. In this article, it is assumed that the absolute values of the positive- and negative-sequence frequencies are equal, i.e., $\omega_{\text{pll}}^{+}+\omega_{\text{pll}}^{-}=0$. Then, the positive-sequence synchronous dynamic equation can be introduced as

$$J_{\text{eq}}^{+}\frac{d\omega_{\text{pll}}^{+}}{dt}=T_{v+}^{*}-T_{v+}-D_{\text{eq}}^{+}\left(\omega_{\text{pll}}^{+}-\omega_{n}\right)$$
$$\begin{cases}J_{\text{eq}}^{+}=\frac{1-k_{\text{p}}L_2I_{td}^{+}+k_pL_3I_t^{-}\cos\left[\left(\delta^{+}+\delta^{-}\right)+\theta_I^{-}\right]}{k_i}\\ D_{\text{eq}}^{+}=\frac{k_p}{k_i}V^{+}\cos\left(\delta^{+}-\phi_1\right)\\ \qquad -L_2I_{td}^{+}+L_3I_t^{-}\cos\left[\left(\delta^{+}+\delta^{-}\right)+\theta_I^{-}\right]\end{cases}\tag{9}$$

where J_{eq}^{+} and D_{eq}^{+} represent the equivalent inertia and damping of the positive-sequence synchronization, respectively.

The modified negative-sequence synchronous dynamic equation is

$$J_{\text{eq}}^{-}\frac{d\omega_{\text{pll}}^{-}}{dt}=T_{v-}^{*}-T_{v-}-D_{\text{eq}}^{-}\left(\omega_{\text{pll}}^{-}+\omega_{n}\right)$$
$$\begin{cases}J_{\text{eq}}^{-}=\frac{1+k_pL_5I_{td}^{-}-k_pL_6I_t^{+}\cos\left[\left(\delta^{+}+\delta^{-}\right)+\theta_I^{+}\right]}{k_{\text{i}}}\\ D_{\text{eq}}^{-}=\frac{k_p}{k_i}V^{-}\cos\left(\delta^{-}+\phi_4\right)+L_5I_{td}^{-}\\ \qquad -L_6I_t^{+}\cos\left[\left(\delta^{+}+\delta^{-}\right)+\theta_I^{+}\right]\end{cases}\tag{10}$$

where J_{eq}^{-} and D_{eq}^{-} represent the equivalent inertia and damping of the negative-sequence synchronization, respectively.

B. Conditions for the Existence of Dual-Sequence Equilibrium Points Considering Dual-Sequence Couplings and Dynamics

The stable operation of the system requires the existence of equilibrium points. The influence of the sequence coupling currents on the existence of the equilibrium points has been illustrated in [9] and [28]. In contrast to [9] and [28], we here further take the different dynamics between the dual-sequence power angles into account.

For the modified positive-sequence synchronous dynamic equation, the positive-sequence equilibrium points are determined by $T_{v+}^{*}=T_{v+}$ given as

$$T_{v+}=V^{+}\sin\left(\delta^{+}-\phi_1\right)\tag{11}$$
$$T_{v+}^{*}=R_2I_{tq}^{+}+\omega_nL_2I_{td}^{+}-R_3I_t^{-}\sin\left[\left(\delta^{+}+\delta^{-}\right)+\theta_I^{-}\right]$$
$$-\omega_nL_3I_t^{-}\cos\left[\left(\delta^{+}+\delta^{-}\right)+\theta_I^{-}\right].\tag{12}$$

For the modified negative-sequence synchronous dynamic equation, the negative-sequence equilibrium points are determined by $T_{v-}^{*}=T_{v-}$ given as

$$T_{v-}=V^{-}\sin\left(\delta^{-}+\phi_4\right)\tag{13}$$
$$T_{v-}^{*}=R_5I_{tq}^{-}+\omega_nL_5I_{td}^{-}-R_6I_t^{+}\sin\left[\left(\delta^{+}+\delta^{-}\right)+\theta_I^{+}\right]$$
$$-\omega_nL_6I_t^{+}\cos\left[\left(\delta^{+}+\delta^{-}\right)+\theta_I^{+}\right].\tag{14}$$

The actual output torque T_{v+} changes with the variation of δ^{+}, and T_{v-} changes with the variation of δ^{-}. It should be noted that the reference values T_{v+}^{*} and T_{v-}^{*} are no longer considered constant values. If $(\delta^{+}+\delta^{-})=0$, T_{v+}^{*} will be expressed by $R_2I_{tq}^{+}+\omega_nL_2I_{td}^{+}-R_3I_{tq}^{-}-\omega_nL_3I_{td}^{-}$, and T_{v-}^{*} will be expressed by $R_5I_{tq}^{-}+\omega_nL_5I_{td}^{-}-R_6I_{tq}^{+}-\omega_nL_6I_{td}^{+}$. With the information of the dual-sequence currents and impedances, the existence of the equilibrium points can be analyzed. However, because $(\delta^{+}+\delta^{-})=0$ is not always true, which has been

$$J_{\text{v}-}^{-}\frac{d\omega_{\text{pll}}^{-}}{dt}+J_{\text{v}-}^{+}\frac{d\omega_{\text{pll}}^{+}}{dt}=T_{\text{v}-}^{*}-T_{\text{v}-}-D_{\text{v}-}^{-}\left(\omega_{\text{pll}}^{-}+\omega_{n}\right)+D_{\text{v}-}^{+}\left(\omega_{\text{pll}}^{+}-\omega_{n}\right)$$
$$\begin{cases}T_{\text{v}-}^{*}=R_5I_{tq}^{-}+\omega_nL_5I_{td}^{-}-R_6I_t^{+}\sin\left[\left(\delta^{+}+\delta^{-}\right)+\theta_I^{+}\right]-\omega_nL_6I_t^{+}\cos\left[\left(\delta^{+}+\delta^{-}\right)+\theta_I^{+}\right]\\ T_{v-}=V^{-}\sin\left(\delta^{-}+\phi_4\right)\\ J_{v-}^{-}=\frac{1+k_pL_5I_{td}^{-}}{k_i}\\ J_{v-}^{+}=\frac{k_p}{k_i}L_6I_t^{+}\cos\left[\left(\delta^{+}+\delta^{-}\right)+\theta_I^{+}\right]\\ D_{v-}^{-}=\frac{k_p}{k_i}V_e^{-}\cos\left(\delta^{-}+\phi_4\right)+L_5I_{td}^{-}+\frac{k_p}{k_i}Z_6I_t^{+}\cos\left[\left(\delta^{+}+\delta^{-}\right)+\theta_I^{+}+\phi_6\right]\\ D_{v-}^{+}=-L_6I_t^{+}\cos\left[\left(\delta^{+}+\delta^{-}\right)+\theta_I^{+}\right]-\frac{k_p}{k_i}Z_6I_t^{+}\cos\left[\left(\delta^{+}+\delta^{-}\right)+\theta_I^{+}+\phi_6\right]\end{cases}\tag{8}$$

confirmed in Section III-A, T^*_{v+} and T^*_{v-} vary along with the variation of $(\delta^+ + \delta^-)$ under asymmetrical grid faults.

Obviously, the reference values will become nonfixed values with time-varying characteristics. To simplify the complexity without losing correctness, the upper to lower limit of the time-varying term is restrained, which is conservative but acceptable.

The coupled time-varying term about $(\delta^+ + \delta^-)$ follows the trigonometric theorem and T^*_{v+} can be rewritten as

$$T^*_{v+} = R_2 I^+_{tq} + \omega_n L_2 I^+_{td} - I^-_t \sqrt{{R_3}^2 + (\omega_n L_3)^2} \sin \left[\left(\delta^+ + \delta^-\right) + \theta^-_I + \alpha\right] \tag{15}$$

where $\alpha = \arccos \frac{R_3}{\sqrt{{R_3}^2 + (\omega_n L_3)^2}}$.

T^*_{v-} can also be rewritten as

$$T^*_{v-} = R_5 I^-_{tq} + \omega_n L_5 I^-_{td} - I^+_{\mathrm{t}} \sqrt{{R_6}^2 + (\omega_n L_6)^2} \times \sin \left[\left(\delta^+ + \delta^-\right) + \theta^+_I + \beta\right] \tag{16}$$

where $\beta = \arccos \frac{R_6}{\sqrt{{R_6}^2 + (\omega_n L_6)^2}}$.

Thus, T^*_{v+} and T^*_{v-} can be determined by the following values:

$$\begin{aligned}&\left[T^*_{v+\min}, T^*_{v+\max}\right] \\ &= \left[R_2 I^+_{tq} + \omega_n L_2 I^+_{td} - I^-_t \sqrt{{R_3}^2 + (\omega_n L_3)^2},\right. \\ &\left. R_2 I^+_{tq} + \omega_n L_2 I^+_{td} + I^-_t \sqrt{{R_3}^2 + (\omega_n L_3)^2}\right] \end{aligned} \tag{17}$$

$$\begin{aligned}&\left[T^*_{v-\min}, T^*_{v-\max}\right] \\ &= \left[R_5 I^-_{tq} + \omega_n L_5 I^-_{td} - I^+_t \sqrt{{R_6}^2 + (\omega_n L_6)^2},\right. \\ &\left. R_5 I^-_{tq} + \omega_n L_5 I^-_{td} + I^+_t \sqrt{{R_6}^2 + (\omega_n L_6)^2}\right]. \end{aligned} \tag{18}$$

The intersections of the two curves T^*_{v+} and T_{v+} exist when T^*_{v+} lies within the upper and lower limits of the sinusoidal curve T_{v+}. The positive-sequence equilibrium points of the system exist when the following equation is satisfied:

$$\left(T^*_{v+\max} \le V^+\right) \cap \left(T^*_{v+\min} \ge -V^+\right). \tag{19}$$

Similarly, the intersections of the two curves T^*_{v-} and T_{v-} exist when T^*_{v-} lies within the upper and lower limits of the sinusoidal curve T_{v-}. The negative-sequence equilibrium points of the system exist when the following equation is satisfied:

$$\left(T^*_{v-\max} \le V^-\right) \cap \left(T^*_{v-\min} \ge -V^-\right). \tag{20}$$

Fig. 7 shows the comparison of the existence of positive-sequence equilibrium points under three different assumptions. For the sake of illustration, positive- and negative-sequence couplings are abbreviated as PNSC. The analysis considers the dynamic of $(\delta^+ + \delta^-)$, and then T^*_{v+} is limited in a given range. It is easy to find that the reference torque has sinusoidal time-varying characteristics when both dual-sequence couplings and dynamics are considered, and its maximum value exceeds the constant reference values for the other two cases, which implies that the judgment of equilibrium points of this article is stricter and more correct.

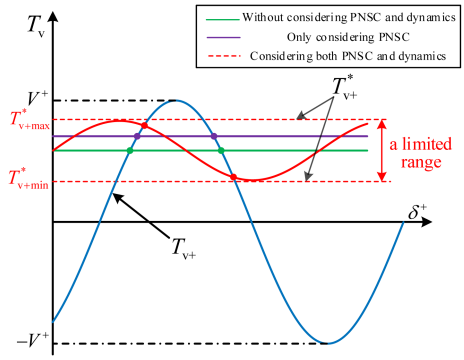

Fig. 7. Comparison of three judgments for the existence of positive-sequence equilibrium points.

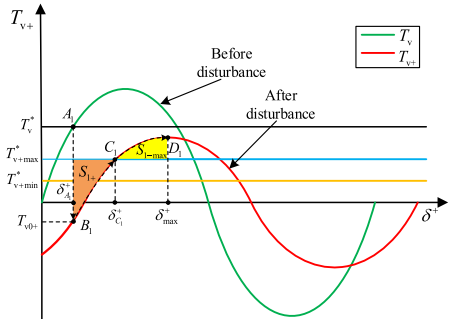

Fig. 8. Motion trajectory of the positive-sequence operating point when $T_{v0+} < T^*_{v+\min} < T^*_{v+\max}$.

C. Transient Process Analysis Based on Equal Area Criterion

Since the dual-sequence synchronous dynamic equations have rotor motion characteristics similar to a synchronous machine, the transient process of the dual-sequence operating points can be analyzed by the equal area criterion [29], [30]. The following is an example of the transient analysis of the positive-sequence synchronization.

To obtain a relatively reliable judgment, the positive-sequence damping should be positive [17], [31]

$$D^+_{\mathrm{eq}} = \frac{k_p}{k_i} V^+ \cos\left(\delta^+ - \phi_1\right) - L_2 I^+_{td} + L_3 I^-_t \cos\left[\left(\delta^+ + \delta^-\right) + \theta^-_I\right] > 0. \tag{21}$$

Thus, $(\delta^+_{\min}, \delta^+_{\max})$ can be given. When $\delta^+ \in (\delta^+_{\min}, \delta^+_{\max})$, the positive-sequence damping is positive.

The actual output torque of the inverter under normal operation is $T_v = V_g \sin(\delta)$. As shown in Fig. 8, the intersection point A_1 is the operating point before the fault. When an asymmetrical grid fault occurs, the equivalent circuit model is changed, with the dual-sequence currents being injected. The actual torque after the fault is $T_{v+} = V^+ \sin(\delta^+ - \varphi_1)$, which is reduced in amplitude and shifted in phase compared to the prefault torque. The reference torque after the fault is $T^*_{v+} \in [T^*_{v+\min}, T^*_{v+\max}]$.

1) $T_{v0+} < T^*_{v+\min} < T^*_{v+\max}$

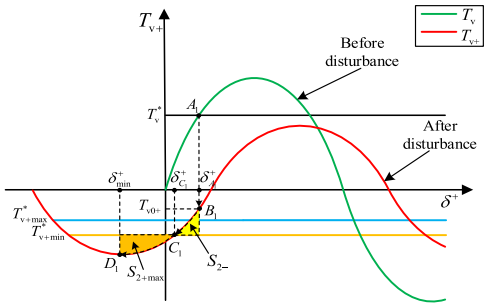

Fig. 9. Motion trajectory of the positive-sequence operating point when $T_{v0+} > T^*_{v+\max} > T^*_{v+\min}$.

In Fig. 8, if the power angle δ^+_{A1} corresponds to the postfault torque T_{v0+}, which is smaller than $T_{v+\min}$, then the new stable equilibrium point will be larger than δ^+_{A1}. When the asymmetrical fault occurs, the operating point directly jumps from A_1 to B_1. It is appropriate to select $T^*_{v+\max}$ as the reference torque because the larger reference will make the system harder to restore stability. During the acceleration process, the operating point moves from B_1 to C_1 due to $T^*_{v+\max} > T_{v+}$ with the increase of ω^+_{pll} and δ^+. Thus, the area of acceleration in this process can be expressed as

$$S_{1+} = \int_{\delta^+_{A_1}}^{\delta^+_{C_1}} \left(T^*_{v+\max} - T_{v+}\right) d\delta. \tag{22}$$

After that, ω^+_{pll} starts to decrease continuously due to $T^*_{v+\max} < T_{v+}$. If the positive-sequence frequency can be reduced below ω_n before D_1, then the operating point will start moving backward and eventually stabilize at C_1 after several oscillations. Otherwise, the operating point will enter the negative damping region, and the positive-sequence frequency may not converge to ω_n. The maximum deceleration area is

$$S_{1-\max} = \int_{\delta^+_{C_1}}^{\delta^+_{\max}} \left(T_{v+} - T^*_{v+\max}\right) d\delta. \tag{23}$$

According to (22) and (23), the basis to ensure transient process stability can be derived

$$S_{1+} \le S_{1-\max}. \tag{24}$$

1) $T_{v0+} > T^*_{v+\max} > T^*_{v+\min}$

In Fig. 9, if the postfault torque T_{v0+} is larger than $T^*_{v+\max}$, then the new stable equilibrium point must be smaller than δ^+_{A1}. In this case, if the positive-sequence synchronization is reached, then the positive-sequence operating point will undergo the process of deceleration and acceleration, and the corresponding transient stability condition is

$$S_{2-} \le S_{2+\max}. \tag{25}$$

The area of deceleration at this stage can be expressed as

$$S_{2-} = \int_{\delta^+_{C_1}}^{\delta^+_{A_1}} \left(T_{v+} - T^*_{v+\min}\right) d\delta. \tag{26}$$

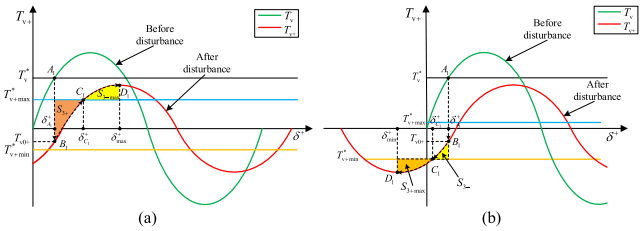

Fig. 10. Motion trajectory of the positive-sequence operating point when $T^*_{v+\min} < T_{v0+} < T^*_{v+\max}$. (a) $T_{v0+}$is far from $T^*_{v+\max}$. (b) T_{v0+} is far from $T^*_{v+\min}$.

The maximum acceleration area can be expressed as

$$S_{2+\max} = \int_{\delta^+_{\min}}^{\delta^+_{C_1}} \left(T^*_{v+\min} - T_{v+}\right) d\delta. \tag{27}$$

1) $T^*_{v+\min} < T_{v0+} < T^*_{v+\max}$

In Fig. 10, if T_{v0+} is located between $T^*_{v+\min}$ and $T^*_{v+\max}$, then the stable condition can be derived according to the distance between T_{v0+} and the two torques. When T_{v0+} is far from $T^*_{v+\max}$, as shown in Fig. 10(a), $T^*_{v+\max}$ is selected as the reference torque, and the new stable equilibrium point will be larger than δ^+_{A1}. It is similar to the analysis of Fig. 8, and the corresponding positive-sequence transient stability condition is

$$S_{3+} \le S_{3-\max}. \tag{28}$$

When T_{v0+} is far from $T^*_{v+\min}$, as shown in Fig. 10(b), $T^*_{v+\min}$ is selected as the reference torque and the new stable equilibrium point will be smaller than δ^+_{A1}. It is similar to the analysis of Fig. 9, and the corresponding positive-sequence transient stability condition is

$$S_{3-} \le S_{3+\max}. \tag{29}$$

D. Judgment for Transient Synchronization Stability

Table III summarizes the judgment for transient synchronization stability under asymmetrical grid faults. For the different values of positive- and negative-sequence reference torques and the corresponding area calculation, the stability of the system can be given, and the reasons for stability or instability are explained. Based on these, the synchronization stability of the system can be assessed.

A flowchart describing how to apply the transient stability method under asymmetrical faults is shown in Fig. 11. First, the parameter update is performed. The synchronization stability of both positive and negative sequences is then assessed, including the existence of dual-sequence equilibrium points and the transient process of dual-sequence operating points.

V. Verifications

A. Simulation Verification

To verify the accuracy of the transient stability method proposed in this article, a grid-tied inverter in Fig. 1 is built in MATLAB/Simulink. A single-phase short-circuit fault occurs on the transmission line between the inverter and the grid to

TABLE III
JUDGMENT FOR TRANSIENT SYNCHRONIZATION STABILITY

Positive-sequence reference torque	Negative-sequence reference torque	States	Causes
$T^*_{v+max} > V^+$ or $T^*_{v+min} < -V^+$	$\left(-V^- \le T^*_{v-min}\right) \cap \left(T^*_{v-max} \le V^-\right)$	Unstable	Without positive-sequence equilibrium points
$\left(-V^+ \le T^*_{v+min}\right) \cap \left(T^*_{v+max} \le V^+\right)$	$T^*_{v-max} > V^-$ or $T^*_{v-min} < -V^-$	Unstable	Without negative-sequence equilibrium points
$\left(-V^+ \le T^*_{v+min}\right) \cap \left(T^*_{v+max} \le V^+\right)$ $T_{v0+} < T^*_{v+min}, S_{1+} \le S_{1-max}$ or $T_{v0+} > T^*_{v+max}, S_{2-} \le S_{2+max}$ or $T^*_{v+min} < T_{v0+} < T^*_{v+max}$, $S_{3-/+} \le S_{3+/-max}$	$\left(-V^- \le T^*_{v-min}\right) \cap \left(T^*_{v-max} \le V^-\right)$ $T_{v0-} < T^*_{v-min}, S_{4+} \le S_{4-max}$ or $T_{v0-} > T^*_{v-max}, S_{5-} \le S_{5+max}$ or $T^*_{v-min} < T_{v0-} < T^*_{v-max}$, $S_{6-/+} \le S_{6+/-max}$	Stable	With equilibrium points, transient process stable

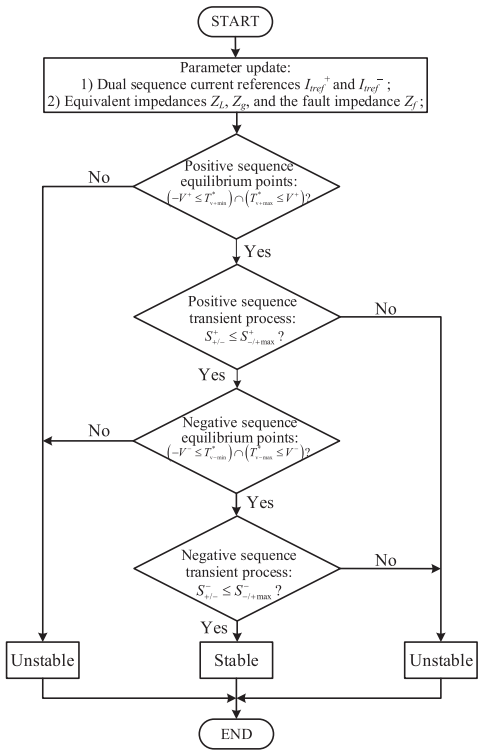

Fig. 11. Flowchart for the application of the transient stability analysis method under asymmetrical grid faults.

TABLE IV
PARAMETERS (SIMULATION)

Symbol	Description	Value
U_{dc}	DC voltage	300 V
V_g	Grid voltage	$100\sqrt{2}$ V
S_N	Rated capacity	30 kVA
ω_n	Rated frequency	100 π rad/s
L_{f1}, L_{f2}, C_f	LCL filter	5 mH, 2 mH, 20 μF
$Z_L^+ = Z_L^- = Z_L^0 / 3$	Z_L impedance	0.05+j0.0942 Ω
$Z_g^+ = Z_g^- = Z_g^0 / 3$	Z_g impedance	0.45+j0.8478 Ω
Z_f	Fault impedance	0.01 Ω
k_{p_PLL}, k_{i_PLL}	PLL PI parameters	10 rad/Vs), 5 rad/Vs^2)
k_{p_Cur}, k_{r_Cur}	Current PR parameters	20 Ω, 2000 Ω/s

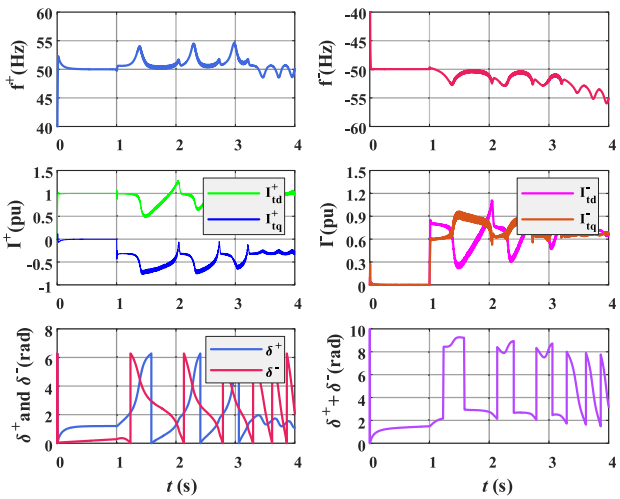

Fig. 12. Simulation results for transient synchronization instability of Case I.

simulate the asymmetrical scenario. Simulation parameters are given in Table IV. The controller gains are provided with appropriate units [32]. Assuming that the fault occurs at 1 s, the inverter starts to regulate dual-sequence currents.

1) Nonexistence of the Equilibrium Points

To support the positive-sequence voltage, the positive-sequence active and reactive currents of the inverter are $I_{td}^+ = 1$ pu and $I_{tq}^+ = -0.3$ pu, and to regulate the negative-sequence voltage, the negative-sequence active and reactive currents are $I_{td}^- = 0.8$ pu and $I_{tq}^- = 0.6$ pu . However, from the simulation results in Fig. 12, it can be found that after 1 s, the positive- and negative-sequence frequencies, active and reactive currents begin to oscillate and diverge, and the dual-sequence power angles begin to oscillate periodically, which indicates that the system appears to be unstable.

According to the conditions for the existence of the dual-sequence equilibrium points proposed in this article, the system

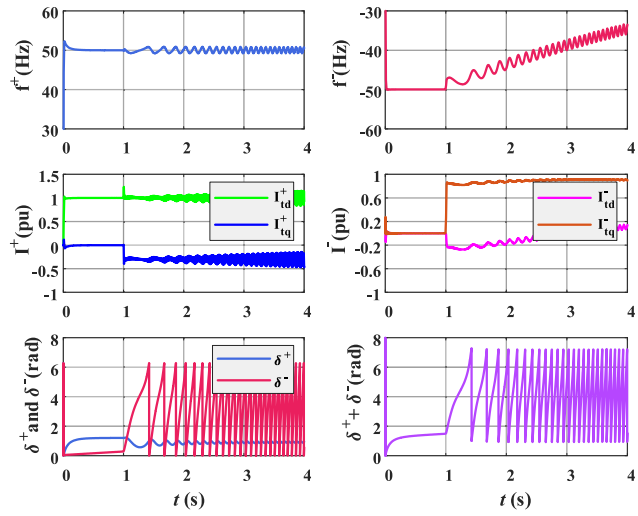

Fig. 13. Simulation results for transient synchronization instability of Case II.

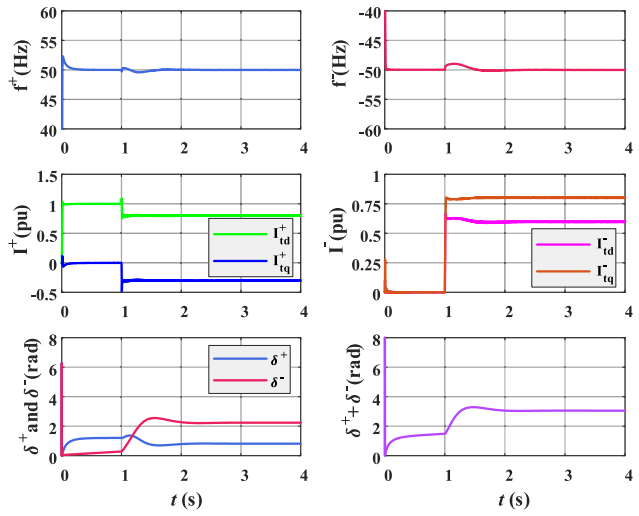

Fig. 14. Simulation results for transient synchronization stability of Case III.

is bound to lose synchronism because the positive- and negative-sequence equilibrium points do not exist at this time.

2) *Poor Dynamic Performance*

To achieve asymmetrical voltage support, the negative-sequence currents are $I_{td}^{-} = -0.3$ pu and $I_{tq}^{-} = 0.8$ pu, and the positive-sequence currents are $I_{td}^{+} = 1$ pu and $I_{tq}^{+} = -0.3$ pu. From Fig. 13, the system is unstable. After 1 s, the positive-sequence frequency starts to oscillate, the negative-sequence frequency directly diverges, and the sum of the dual-sequence power angles appears to oscillate periodically.

The reason is that although the dual-sequence equilibrium points of the system exist, according to the transient process stability conditions in this article, $S_{1+} = 6.93 > 5.56 = S_{1-\max}$, the system cannot keep stable.

3) *Transient Synchronous Stabilization*

When the positive-sequence active and reactive currents are $I_{td}^{+} = 1$ pu and $I_{tq}^{+} = -0.3$ pu and the negative-sequence active and reactive currents are $I_{td}^{-} = 0.8$ pu and $I_{tq}^{-} = 0.6$ pu, as shown in Fig. 14, the system keeps the transient stable after suffering the fault. Compared with 1) and 2), the dual-sequence frequencies are basically stable at 50 Hz and -50 Hz. The dual-sequence currents achieve fast and accurate tracking of the reference values, and the dual-sequence power angles remain stable.

According to the transient stability judgment in this article, considering the couplings of dual-sequence currents and the dynamic effect of the power angles, the system at this time has equilibrium points and superior dynamic performance. As a result, the transient synchronization stability is maintained.

4) *Comparison of Transient Stability Under Different Criteria*

The conventional methods can be classified into the following three types. One is not considering the existence of dual-sequence coupling currents [10], [11], and the other is not taking

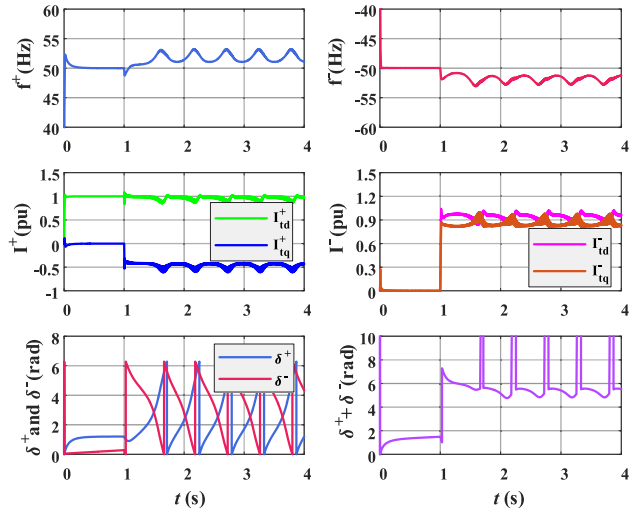

Fig. 15. Simulation results for transient synchronization instability of Case IV.

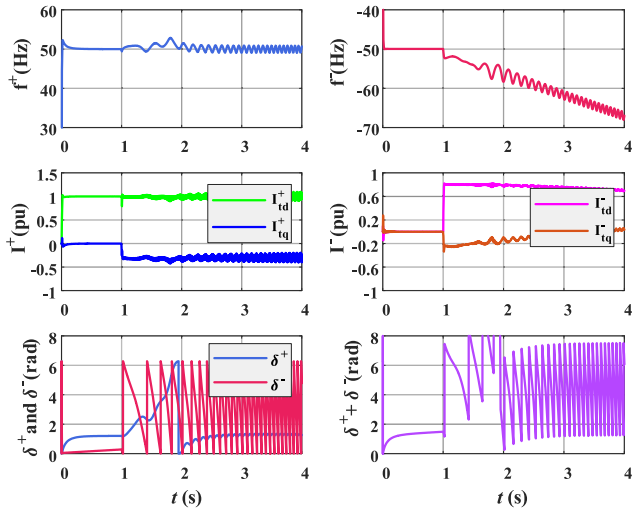

Fig. 16. Simulation results for transient synchronization instability of Case V.

TABLE V
SIMULATION COMPARISON OF SYNCHRONIZATION STABILITY ANALYSIS METHODS

Grid faults	Cases	Coupling degree γ_1	Coupling degree γ_2	Sum of power angles	Without considering PNSC and dynamics [10], [11]	Only considering PNSC [12], [13]	Proposed method	Actual system stability
	I	46.32%	40.16%	/	Stable	Unstable	Unstable	Unstable
SLG	II	42.43%	84.86%	/	Stable	Stable	Unstable	Unstable
	III	53.13%	37.43%	3.25rad	Unstable	Stable	Stable	Stable
	IV	53.97%	35.21%	/	Stable	Unstable	Unstable	Unstable
DLG	V	40.73%	53.38%	/	Stable	Stable	Unstable	Unstable
	VI	55.65%	37.19%	6.08rad	Stable	Stable	Stable	Stable

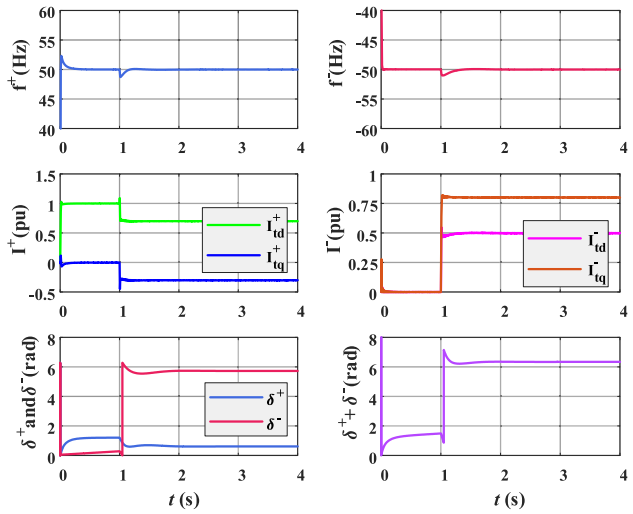

Fig. 17. Simulation results for transient synchronization instability of Case VI.

into account the dynamic effect of the dual-sequence power angles [12], [13]. By contrast, the proposed transient stability method in this article considers the couplings of dual-sequence currents and the dynamic effect of dual-sequence power angles at the same time.

Based on these methods, the transient stability of the system can be predicted. The stability results judged by these methods for the three cases, i.e., Case I, Case II, and Case III, are shown in Table V. To show the coupling impacts of the dual-sequence currents, two coupling degrees γ_1 and γ_2 are defined as

$$\gamma_1 = \frac{I_{\mathrm{t}}^{-}\sqrt{{R_3}^2 + (\omega_{\mathrm{n}} L_3)^2}}{R_2 I_{\mathrm{tq}}^{+} + \omega_{\mathrm{n}} L_2 I_{\mathrm{td}}^{+} + I_{\mathrm{t}}^{-}\sqrt{{R_3}^2 + (\omega_{\mathrm{n}} L_3)^2}} \tag{30}$$

$$\gamma_2 = \frac{I_{\mathrm{t}}^{+}\sqrt{{R_6}^2 + (\omega_{\mathrm{n}} L_6)^2}}{R_5 I_{\mathrm{tq}}^{-} + \omega_{\mathrm{n}} L_5 I_{\mathrm{td}}^{-} + I_{\mathrm{t}}^{+}\sqrt{{R_6}^2 + (\omega_{\mathrm{n}} L_6)^2}} \tag{31}$$

where γ_1 denotes the proportion of the negative-sequence coupling component and γ_2 denotes the proportion of the positive-sequence coupling component. In addition, the sum of the positive- and negative-sequence power angles if the system remains stable is shown in Table V. In Case I and Case II, the dual-sequence power angles oscillate due to the instability.

In addition, the asymmetrical scenario of DLG is supplemented. Figs. 15–17 show simulation results for transient stability when DLG fault occurs. The comparison of the proposed method and the conventional methods in terms of predicted stability under SLG and DLG faults is presented in Table V. By comparing the results of the three transient stability judgments, the proposed method is verified to give accurate stability results of the actual system in all cases. It can guide how to constrain the dual-sequence currents to ensure the stable ride-through of the asymmetrical fault.

Since our current work focuses on the synchronization stability of the inverter, the power grid is modeled as a voltage source with an impedance in series. Hence, the asymmetrical grid faults are assumed by the unbalanced voltages of the source and the varying impedance. A similar model of grid faults in transient stability evaluation is widely employed [9], [10], [11], [12], [13], and it is believed to be feasible in stability prediction in most cases.

B. Experimental Verification

Multiple sets of experiments under single-phase ground fault are carried out on the hardware platform in Fig. 18 to validate the effectiveness of the proposed method. The experimental parameters are shown in Table VI. The ac grid is simulated with a grid simulator (PSA6006-3-Pro). The grid-following inverter is powered by a dc power supply (BTLA-PMA006-A011-MI) and uses MOSFETs (IPW60R099C6) as switching divers. A Texas Instruments DSP28335 digital signal processor performs the dual-sequence current injection algorithm to control the switching of the MOSFETs. An oscilloscope (ROGOL MSO5354) and Code Composer Studio are used to record the experimental waveforms of voltage, current, power angle, and frequency.

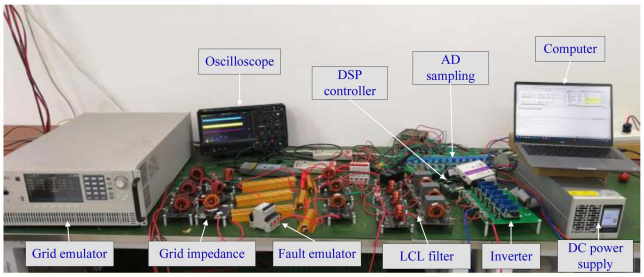

Fig. 18. Hardware platform for a grid-following inverter.

TABLE VI
PARAMETERS (EXPERIMENT)

Symbol	Description	Value
U_{dc}	DC voltage	70 V
V_g	Grid voltage	$15\sqrt{2}$ V
ω_n	Rated frequency	100π rad/s
L_{f1}, L_{f2}, C_f	LCL filter	3 mH, 1.92 mH, 30 μF
$Z_L^+ = Z_L^- = Z_L^0/3$	Z_L impedance	0.5+j0.314 Ω
$Z_g^+ = Z_g^- = Z_g^0/3$	Z_g impedance	3+j1.884 Ω
Z_f	Fault impedance	0.001 Ω
k_{p_PLL}, k_{i_PLL}	PLL PI parameters	50 rad/Vs), 10 rad/Vs^2)
k_{p_Cur}, k_{r_Cur}	Current PR parameters	12.5 Ω, 2000 Ω/s

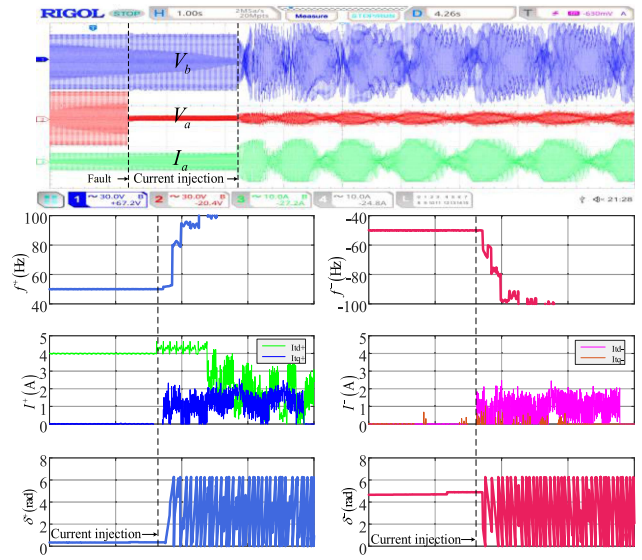

Fig. 19. Experimental results for transient synchronization instability of Case VII: $I_{td}^+ = 4$ A, $I_{tq}^+ = 4$ A, $I_{td}^- = 3$ A, and $I_{tq}^- = 3$ A.

Figs. 19–21 show the actual voltages, currents, dual-sequence frequencies, and power angles of the system after three forms of dual-sequence current injection in accordance with different requirements of asymmetrical voltage support, in which phase a serves as the faulted phase and phase b serves as the nonfaulted phase.

In Fig. 19, the dual-sequence frequencies diverge rapidly, the dual-sequence currents cannot track the reference values,

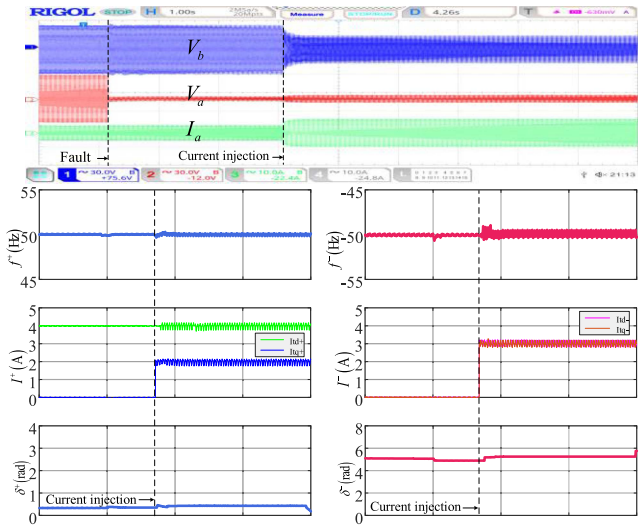

Fig. 20. Experimental results for transient synchronization instability of Case VIII: $I_{td}^+ = 4$ A, $I_{tq}^+ = 2$ A, $I_{td}^- = 3$ A, and $I_{tq}^- = 3$ A.

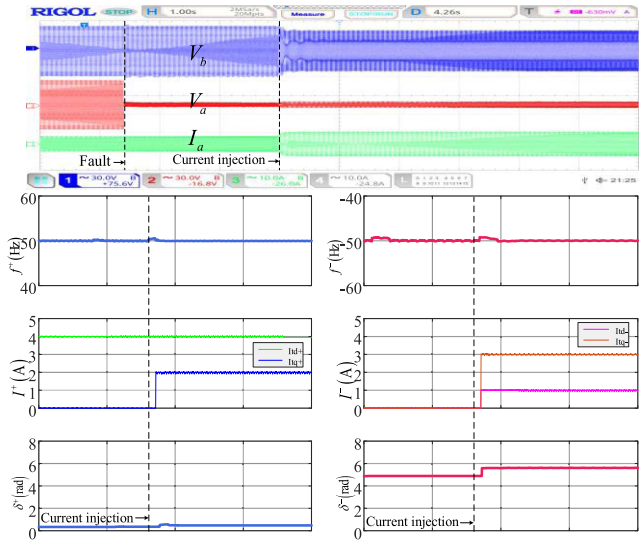

Fig. 21. Experimental results for transient synchronization stability of Case IX: $I_{td}^+ = 4$ A, $I_{tq}^+ = 2$ A, $I_{td}^- = 1$ A, and $I_{tq}^- = 3$ A.

the dual-sequence power angles oscillate periodically, and the system actually exhibits instability. In Fig. 20, the dual-sequence frequencies oscillate in a wide range, the dual-sequence currents oscillate near the reference value, and the system exhibits critical instability. In Fig. 21, the positive- and negative-sequence frequencies are stable near 50 Hz and -50 Hz, respectively, the dual-sequence currents are accurately tracked, and the system remains stable.

Table VII shows the determination results of these experimental cases under three stability criteria. It can be found that the proposed method results, which simultaneously consider the dual-sequence current couplings and the power angle difference, match well with the real states of the system. Therefore, the accuracy and superiority of the synchronization stability method proposed in this article are confirmed.

TABLE VII
EXPERIMENT COMPARISON OF SYNCHRONIZATION STABILITY ANALYSIS METHODS

Cases	Coupling degree γ_1	Coupling degree γ_2	Sum of power angles	Without considering PNSC and dynamics [10], [11]	Only considering PNSC [12], [13]	Proposed method	Actual system stability
VII	28.99%	42.06%	/	Stable	Unstable	Unstable	Unstable
VIII	37.09%	33.5%	/	Stable	Stable	Unstable	Unstable
IX	30.41%	40.41%	5.83 rad	Stable	Stable	Stable	Stable

VI. CONCLUSION

In this article, a dual-sequence dynamic coupling model of grid-following inverters during asymmetrical grid faults is presented for synchronization stability analysis. Compared to the previous studies, the proposed method has the following merits.

1) The developed dual-sequence synchronous model takes into consideration not only the coupling effects of dual-sequence currents but also the dynamic effects caused by the difference of dual-sequence power angles.
2) The previous studies do not consider the current couplings or power angle differences, which are proven to give inaccurate judgments.
3) It is pointed out that when asymmetrical faults occur far from the infinite bus, interaction couplings of the positive and the negative sequences are large. It is revealed that dual-sequence couplings cannot be ignored, and this article's method is more accurate than previous methods.

Our future work will focus on synchronization stability analysis of multi-inverters with multioperating points during asymmetrical faults.

REFERENCES

[1] F. Blaabjerg, R. Teodorescu, M. Liserre, and A. V. Timbus, "Overview of control and grid synchronization for distributed power generation systems," *IEEE Trans. Ind. Electron.*, vol. 53, no. 5, pp. 1398–1409, Oct. 2006.

[2] J. Rocabert, A. Luna, F. Blaabjerg, and P. Rodríguez, "Control of power converters in ac microgrids," *IEEE Trans. Power Electron.*, vol. 27, no. 11, pp. 4734–4749, Nov. 2012.

[3] Y. Li, Y. Gu, and T. C. Green, "Revisiting grid-forming and grid-following inverters: A duality theory," *IEEE Trans. Power Syst.*, vol. 37, no. 6, pp. 4541–4554, Nov. 2022.

[4] S. Mortazavian, M. M. Shabestary, and Y. A.-R. I. Mohamed, "Analysis and dynamic performance improvement of grid-connected voltage–source converters under unbalanced network conditions," *IEEE Trans. Power Electron.*, vol. 32, no. 10, pp. 8134–8149, Oct. 2017.

[5] L. He, Z. Shuai, X. Zhang, X. Liu, Z. Li, and Z. J. Shen, "Transient characteristics of synchronverters subjected to asymmetric faults," *IEEE Trans. Power Del.*, vol. 34, no. 3, pp. 1171–1183, Jun. 2019.

[6] VDE VERLAG GmbH, "Technical requirements for the connection and operation of customer installations to the high voltage network," VDE VERLAG GmbH, Berlin, Germany, VDE-AR-N 4120, 2018.

[7] X. Li et al., "The largest estimated domain of attraction and its applications for transient stability analysis of PLL synchronization in weak-grid-connected VSCs," *IEEE Trans. Power Syst.*, vol. 38, no. 5, pp. 4107–4121, Sep. 2023.

[8] C. He, X. He, H. Geng, H. Sun, and S. Xu, "Transient stability of low-inertia power systems with inverter-based generation," *IEEE Trans. Energy Convers.*, vol. 37, no. 4, pp. 2903–2912, Dec. 2022.

[9] X. He, C. He, S. Pan, H. Geng, and F. Liu, "Synchronization instability of inverter-based generation during asymmetrical grid faults," *IEEE Trans. Power Syst.*, vol. 37, no. 2, pp. 1018–1031, Mar. 2022.

[10] M. G. Taul, S. Golestan, X. Wang, P. Davari, and F. Blaabjerg, "Modeling of converter synchronization stability under grid faults: The general case," *IEEE J. Emerg. Sel. Topics Power Electron.*, vol. 10, no. 3, pp. 2790–2804, Jun. 2022.

[11] X. Li, Z. Wang, L. Zhu, L. Guo, and C. Wang, "Analytical dual-sequence current injections feasible region of weak-grid connected VSC under asymmetric grid faults," *IEEE Trans. Power Syst.*, vol. 38, no. 6, pp. 5546–5559, Nov. 2023.

[12] Y. Luo et al., "Transient synchronous stability analysis and enhancement control strategy of a PLL-based VSC system during asymmetric grid faults," *Protection Control Mod. Power Syst.*, vol. 8, no. 2, pp. 1–17, Apr. 2023.

[13] Y. Li, C. Lin, J. Hu, and J. Guo, "PLL synchronization stability of grid-connected VSCs under asymmetric ac faults," *IEEE Trans. Energy Convers.*, vol. 37, no. 4, pp. 2438–2448, Dec. 2022.

[14] A. Camacho, M. Castilla, J. Miret, A. Borrell, and L. G. de Vicuña, "Active and reactive power strategies with peak current limitation for distributed generation inverters during unbalanced grid faults," *IEEE Trans. Ind. Electron.*, vol. 62, no. 3, pp. 1515–1525, Mar. 2015.

[15] M. Islam, M. Nadarajah, and M. J. Hossain, "A grid-support strategy with PV units to boost short-term voltage stability under asymmetrical faults," *IEEE Trans. Power Syst.*, vol. 35, no. 2, pp. 1120–1131, Mar. 2020.

[16] H. Wu and X. Wang, "Design-oriented transient stability analysis of PLL-synchronized voltage-source converters," *IEEE Trans. Power Electron.*, vol. 35, no. 4, pp. 3573–3589, Apr. 2020.

[17] X. He, H. Geng, J. Xi, and J. M. Guerrero, "Resynchronization analysis and improvement of grid-connected VSCs during grid faults," *IEEE J. Emerg. Sel. Topics Power Electron.*, vol. 9, no. 1, pp. 438–450, Feb. 2021.

[18] P. Hu, Z. Chen, Y. Yu, and D. Jiang, "On transient instability mechanism of PLL-based VSC connected to a weak grid," *IEEE Trans. Ind. Electron.*, vol. 70, no. 4, pp. 3836–3846, Apr. 2023.

[19] Q. Hu, L. Fu, F. Ma, and F. Ji, "Large signal synchronizing instability of PLL-based VSC connected to weak ac grid," *IEEE Trans. Power Syst.*, vol. 34, no. 4, pp. 3220–3229, Jul. 2019.

[20] Y. Ding, F. Gao, and M. M. Khan, "Transient stability analysis of microgrid considering impact of grid-following converter's current controller," *IEEE Trans. Power Electron.*, vol. 39, no. 8, pp. 9100–9105, Aug. 2024.

[21] R. Liu, J. Yao, P. Sun, J. Pei, H. Zhang, and Y. Zhao, "Complex impedance-based frequency coupling characteristics analysis of DFIG-based WT during asymmetric grid faults," *IEEE Trans. Ind. Electron.*, vol. 68, no. 9, pp. 8274–8288, Sep. 2021.

[22] J. Zhao, M. Huang, and X. Zha, "Nonlinear analysis of PLL damping characteristics in weak-grid-tied inverters," *IEEE Trans. Circuits Syst. II, Exp. Briefs*, vol. 67, no. 11, pp. 2752–2756, Nov. 2020.

[23] J. Zhao, M. Huang, H. Yan, C. K. Tse, and X. Zha, "Nonlinear and transient stability analysis of phase-locked loops in grid-connected converters," *IEEE Trans. Power Electron.*, vol. 36, no. 1, pp. 1018–1029, Jan. 2021.

[24] H. Geng, L. Liu, and R. Li, "Synchronization and reactive current support of PMSG-based wind farm during severe grid fault," *IEEE Trans. Sustain. Energy.*, vol. 9, no. 4, pp. 1596–1604, Oct. 2018.

[25] Y. Liu et al., "Transient stability enhancement control strategy based on improved PLL for grid connected VSC during severe grid fault," *IEEE Trans. Energy Convers.*, vol. 36, no. 1, pp. 218–229, Mar. 2021.

[26] R. Ma, J. Li, J. Kurths, S. Cheng, and M. Zhan, "Generalized swing equation and transient synchronous stability with PLL-based VSC," *IEEE Trans. Energy Convers.*, vol. 37, no. 2, pp. 1428–1441, Jun. 2022.

[27] X. Wang, M. G. Taul, H. Wu, Y. Liao, F. Blaabjerg, and L. Harnefors, "Grid-synchronization stability of converter-based resources—An overview," *IEEE Open J. Ind. Appl.*, vol. 1, pp. 115–134, 2020.

[28] Z. Wang et al., "PLL synchronization transient stability analysis of a weak-grid connected VSC during asymmetric faults," *IEEE Trans. Power Electron.*, vol. 39, no. 2, pp. 2140–2154, Feb. 2024.
[29] X. Li, Z. Tian, X. Zha, P. Sun, Y. Hu, and M. Huang, "An iterative equal area criterion for transient stability analysis of grid-tied converter systems with varying damping," *IEEE Trans. Power Syst.*, vol. 39, no. 1, pp. 1771–1784, Jan. 2024.
[30] Y. Tang, Z. Tian, X. Zha, X. Li, M. Huang, and J. Sun, "An improved equal area criterion for transient stability analysis of converter-based microgrid considering nonlinear damping effect," *IEEE Trans. Power Electron.*, vol. 37, no. 9, pp. 11272–11284, Sep. 2022.
[31] X. He, H. Geng, R. Li, and B. C. Pal, "Transient stability analysis and enhancement of renewable energy conversion system during LVRT," *IEEE Trans. Sustain. Energy.*, vol. 11, no. 3, pp. 1612–1623, Jul. 2020.
[32] M. G. Taul, C. Wu, and F. Blaabjerg, "Optimal controller design for transient stability enhancement of grid-following converters under weak-grid conditions," *IEEE Trans. Power Electron.*, vol. 36, no. 9, pp. 10251–10264, Sep. 2021.

Jingrong Yu received the B.S. degree in automation and the Ph.D. degree in control science and engineering from Hunan University, Changsha, China, in 2004 and 2009, respectively.

In 2009, she joined Central South University, Changsha, China, where she is currently an Associate Professor. Her research interests include modeling and control of power electronic converters in renewable energy systems and bidirectional inductive wireless power transfer systems.

Wenhao Yang received the B.S. degree in electrical engineering and automation from Wuhan University of Science and Technology, Wuhan, China, in 2022. He is currently working toward the M.S. degree in electrical engineering with Central South University, Changsha, China.

His research interests include control, stability analysis, and power quality of grid-connected inverters.

Jiaqi Yu was born in Liaoning, China, in 1989. She received the B.S. degree in electrical engineering from North University of China, Taiyuan, China, in 2011, and the Ph.D. degree in electrical engineering from Hunan University, Changsha, China, in 2018.

Since 2019, she has been a Lecturer of Electrical Engineering with Changsha University, Changsha, China. Her research interests include renewable energy systems and transient synchronization stability.

Chen Peng received the B.S. degree in electrical engineering and automation in 2022 from the School of Automation, Central South University, Changsha, China, where he is currently working toward the M.S. degree in electrical engineering.

His research interests include control and grid impedance estimation of grid-connected inverters.

Tingyi Jiang received the B.S. degree in electrical engineering and automation in 2022 from the School of Automation, Central South University, Changsha, China, where he is currently working toward the M.S. degree in electrical engineering.

His research interests include control and parameter estimation of bidirectional inductive wireless power transfer systems in power electronics.

Hankang Tian received the B.S. degree in electrical engineering and automation from the School of Automation, Central South University, Changsha, China, in 2022, where he is currently working toward the M.S. degree in electrical engineering.

His research interests include grid-connected inverter control and grid frequency support.